

Kinematics of a two-dimensional granular Couette experiment at the transition to shearing

C. T. Veje*

PMMH, Ecole Supérieure de Physique et de Chimie Industrielle, 10 Rue Vauquelin, 75231 Paris Cedex 05, France

Daniel W. Howell and R. P. Behringer

Department of Physics and Center for Nonlinear and Complex Systems, Duke University, Durham, North Carolina 27708-0305

(Received 2 June 1998)

We describe experiments on a two-dimensional granular Couette system consisting of photoelastic disks undergoing slow shearing. The disks rest on a smooth surface and are confined between an inner wheel and an outer ring. Only shearing from the inner wheel is considered here. We obtain velocity, particle rotation rate (spin), and density distributions for the system by tracking positions and orientations of individual particles. At a characteristic packing fraction, $\gamma_c \approx 0.77$, the wheel just engages the particles. In a narrow range of γ , $0.77 \leq \gamma \leq 0.80$ the system changes from just able to shear to densely packed. The transition at γ_c has a number of hallmarks of a critical transition, including critical slowing down, and an order parameter. For instance, the mean stress grows from 0 as γ increases above γ_c , and hence plays the role of an order parameter. Also, the mean particle velocity vanishes at the transition point, implying slowing down at γ_c . Above γ_c , the mean azimuthal velocity decreases roughly exponentially with distance from the inner shearing wheel, and the local packing fraction shows roughly comparable exponential decay from a highly dilated region next to the wheel to a denser but frozen packing further away. Approximate but not perfect shear rate invariance occurs; variations from perfect rate invariance appear to be related to small long-time rearrangements of the disks. The characteristic width of the induced “shear band” near the wheel varies most rapidly with distance from the wheel for $\gamma \approx \gamma_c$, and is relatively insensitive to the packing fraction for the larger γ 's studied here. The mean particle spin oscillates near the wheel, and falls rapidly to zero away from the shearing surface. The distributions for the tangential velocity and particle spins are wide and show a complex shape, particularly for the disk layer nearest to the shearing surface. The two-variable distribution function for tangential velocity and spin reveals a separation of the kinematics into a slipping state and a nonslipping state consisting of a combination of rolling and translation. [S1063-651X(99)06001-8]

PACS number(s): 81.05.Rm, 45.05.+x

I. INTRODUCTION

The pioneering work of Reynolds in 1885 [1] and the more elaborate investigations by Bagnold [2] were among the first experiments to closely address the problem of granular shearing. Recently, granular flows in which shearing plays a key role have regained much interest in the physics community. Examples of these flows include pipe and chute flow [4,5], avalanches [6,7], compression [8], and to some extent, convection [3]. In addition, there are interesting connections between granular flows and crack formation and earthquakes [9]. For a recent overview on the general physics of granular media see Jaeger, Nagel and Behringer [10], Behringer and Jenkins [11], and Luding and Herrmann [12].

Here, we study both the mean and statistical kinetic properties of slow shear flow in a two-dimensional (2D) Couette cell filled with photoelastic polymer disks. Using particle tracking techniques, we measure the spin, defined below, transport velocities, and the associated density variations during steady-state shearing. Because the particles are photoelastic, it is also possible to deduce information on the stress state of the system, a topic that we will consider elsewhere [13].

In the traditional picture of shearing for a dense granular material, grains are assumed to be relatively hard. If shear is applied to a sample subject by a normal load, the system responds elastically (if the individual grains are not infinitely stiff) up to the yield point. At the yield point, the system dilates enough to allow shear displacement, resulting in grains slipping over each other. This picture is referred to as Reynolds dilatancy. The dilation often occurs in narrow spatial regions known as shear bands. After the initial dilation, it is generally assumed that the system can attain a steady state under continued shearing without significant temporal variation [14].

In the present experiments, we consider the evolution of the system both during the initial dilation process and for extended times thereafter. The initial stage in this process is the dilation of the material near the shearing wheel. We find that after the formation of this dilated region, the system approaches an approximately statistically stationary state, but that fluctuations can be large. Also, there are indications that some changes in the system continue to occur even over very long times.

Previous experiments on granular shearing have primarily focused on the mean properties of the system. Typical examples include triaxial tests where localized shear bands are formed upon failure of the material [15,16], or shearing in annular cells where shear bands are formed by imposing a moving boundary for unlimited shearing [17–19]. (See also Savage [20] and references therein.) Other experiments have

*Present address: Center for Chaos and Turbulence Studies, Niels Bohr Institute, Blegdamsvej 17, DK-2100 Copenhagen Ø, Denmark.

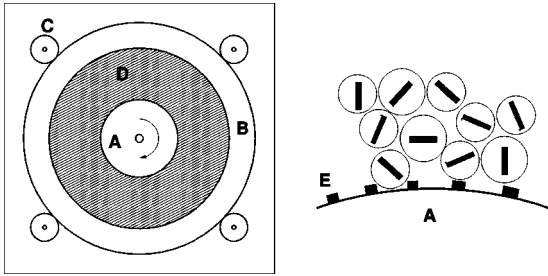


FIG. 1. Left: schematic top view of the experimental setup. Right: schematic drawing of the disks close to the inner shearing wheel.

explored the kinematics of shear zones for fast collisional flows; for example, flow in inclined or vertical chutes and pipes [4,5,7,21]. There have been a number of studies of 2D systems, and of these, the most closely related work to ours is that of Buggisch [22], who investigated mixing mechanisms due to shearing in a 2D annular cell roughly similar to the one described in this paper.

There are also numerical studies involving shearing; these typically center on the stress characteristics of the material [23,24]. However, Schöllmann, Luding and Herrmann [25] have recently performed molecular-dynamics (MD) simulations to investigate the kinematic and force properties on a model system that was structured to be as parallel as possible to the physical system discussed here. A comparison between this model and the present experiment will be presented elsewhere [26].

II. EXPERIMENTAL SETUP AND PROCEDURE

The apparatus, as sketched in Fig. 1, consists of an inner shearing wheel (A) of diameter $D=20.32$ cm and an outer shearing ring (B) of inner diameter 50.8 cm confined by planetary gears (C). Flat, 6-mm-thick disks (region D) are confined between the ring, the wheel, and two smooth horizontal Plexiglas sheets. The separation between the Plexiglas sheets is 2 mm greater than the thickness of the disks, so that there will be no vertical compression of the disks while still allowing little movement out of the plane. The side of the wheel and the inner surface of the ring are coated with plastic “teeth” spaced 0.7 cm apart and 0.2 cm deep (E). Both the wheel and the outer ring can be used to shear, although here we focus on shearing with the inner wheel. The surfaces of the Plexiglas sheets are covered with a fine powder (baking powder) that serves as a nonliquid lubricant. There is still some remaining friction between the disks and sheet, but the friction force is typically at least an order of magnitude smaller than the force in a stress chain [13]. The disks are made of a transparent photoelastic polymer, nominal Young’s modulus, $Y=4.8$ MPa, and these disks are softer than the Plexiglas shearing wheel and ring (nominal Young’s modulus $Y\sim 3$ GPa). Forces in the experiment are not sufficient to cause any appreciable deformation of the disks out of the plane. Each disk has a small dark bar on top which allows us to track the individual disks using conventional video. Frame-grabbed images are analyzed to find each bar and its orientation. Using computer analysis, we follow the trajectories of particles from frame to frame, determining kinematic quantities for each disk, specifically, the azimuthal

velocity V_θ , the radial velocity V_r and the spin S . Here, S corresponds to the angular rotation of a disk in a frame that moves with the disk center of mass and has a fixed orientation relative to a lab coordinate system. The subscripts r and θ refer to a polar coordinate system with the origin at the center of the inner shearing wheel. Throughout this work, we subtract the wheel radius from r , so that $r=0$ corresponds to the location of the wheel edge. By V_θ , we mean the azimuthal angular velocity, $\dot{\theta}$ of the center of a grain. The most interesting quantities are V_θ and S as functions of r ; it is these quantities that we present below. V_r is typically much smaller than V_θ because the grains are largely confined in the radial direction, and we do not consider V_r here.

In these experiments, a bimodal distribution of disks was used, with roughly 400 larger disks of diameter 0.9 cm, and roughly 2500 smaller disks of diameter 0.74 cm. An inhomogeneous distribution is useful, since it limits the formation of hexagonally ordered regions over large scales. One concern was that the disks would segregate by size. However, we did not observe any tendency for this to happen over the course of a typical experiment. We use the diameter d of the smaller disks as a characteristic length scale.

The packing fraction γ (fractional area occupied by disks versus total area) was varied over the range $0.77\leq\gamma\leq 0.80$. As we varied γ , we maintained the ratio of small to large disks roughly constant. We also varied the rotation period, τ of the inner wheel over the range $10^2\text{ s}\leq\tau\leq 2\times 10^3\text{ s}$. This period defines a shear rate, $\Omega=2\pi/\tau$.

After placing the disks in the experiment, but before beginning to take data, we typically ran the inner wheel for ~ 60 min. This corresponded to about 20 rotations of the inner wheel and was necessary, because as a consequence of shearing the local packing fraction γ became nonuniform radially, i.e., a shear band formed, as shown in Fig. 2. Much of the evolution of the resulting shear band occurred in less than a wheel revolution and after ~ 5 rotations the mean density distributions were usually well established. However, some evolution of the density was observed on rare occasions after much longer times.

The transient time for the formation of the shear band also depended on γ . In fact, there are actually two slow times, one associated with the transition between shearing and non-shearing at a critical γ_c , discussed below, and the other associated with long-time rearrangements of a dense packing of grains, and therefore to the parking problem [27,28].

To obtain distributions for V_θ and S , we observed a region of the apparatus that covered roughly 1/4 to 1/5 of the azimuthal span, and all of the radial range. Typically, we observed for times long enough to accumulate $>10^5$ velocity and spin samples over the complete azimuthal and radial span. Typically, this corresponded to ~ 5 rotations of the shearing wheel. Spatial information on all quantities was determined by binning radially (with a bin width $\sim d$); all the data within a radial bin were placed together without regard to the azimuthal coordinate.

It is also important to determine the local packing fraction. We measured this quantity by using the fact that “black light,” i.e., fluorescent light with a largely blue color, was strongly attenuated by the polymer disks. Specifically, the local transmission was determined by the open space. We

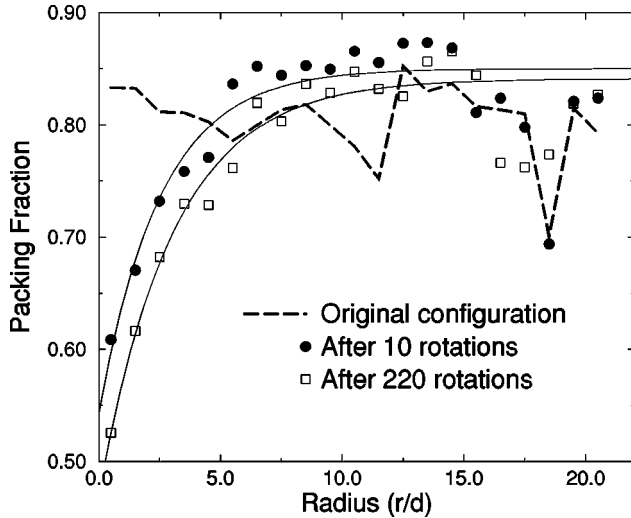


FIG. 2. Results for the local packing fraction after 10 and 220 rotations. The dashed line is the initial configuration. In this case, $\gamma=0.788$. Solid curves show least squares fits to the form $\rho=A-B \exp(-Cr/d)$. Since we are only looking at a quarter of the total cell the area under each curve need not be the same. Most of the relaxation has occurred after 10 rotations; the coefficient C is essentially the same for 10 and 220 rotations. Notably, however, some variation in the packing structure at large r (filling the gap in density near $r=18$) occurred even after very long times—between 20 and 40 rotations—corresponding to a displacement of the shearing wheel by ~ 2200 to ~ 4400 disk diameters.

calibrated this transmission by measurements through various packings of predetermined γ . We estimate that errors associated with these measurements are roughly 1%–2%. We resolve relative changes in packing fraction exactly, since we remove or add exactly known numbers of disks.

To the extent that the shearing rate Ω is small compared to relaxation rates for the system, we would expect rate invariance. In the results presented below, we use normalized units V_θ/Ω for velocity. Then, rate invariance is manifest if data for different Ω , but otherwise similar conditions, are indistinguishable. In the same spirit, we normalize S by $\Omega D/d$, which is the gear-ratio factor for rolling of the disks on the shear wheel.

III. RESULTS

A. Packing fraction profiles

We consider now the density or packing fraction profile, the kinematic distributions, and their means. We begin with the local packing fraction profiles and their time evolution. Figure 2 shows typical results for the local packing fraction as a function of the distance to the shearing wheel. The profiles clearly indicate a dilated region close to the inner wheel. To obtain a characteristic measure of the width of the dilated region we fit the data for $r/d < 14$ to the form $\rho=A-B \exp(-Cr/d)$, where A , B , and C are fit coefficients. Results are shown for the initial state, after 10 rotations and after 220 rotations.

The process of dilation begins with the motion of disks adjacent to the shearing wheel, where yield/failure begins. As time evolves, the density in the vicinity of the failure region decreases, leading to azimuthal flow further from the shearing wheel, and the evolution of a shear band. The angle

through which the inner wheel must rotate, or more usefully, the number of disk diameters traversed, is surprisingly large. Several wheel rotations are necessary to reasonably approach the steady-state profile, (with more than $10^2 d$ per wheel rotation). Thus, in many settings where shear bands evolve, the result may actually be a transient rather than the steady state. The nature and length of this transient is interesting, since it relates to failure in other granular flows and possibly to situations such as earthquake fault zones.

Clearly the effect of continued shearing for more than 10 rotations is small. For the most part, the structure far from the shearing wheel remains largely frozen. However, there can be changes in the packing at large r/d that impact other features of the flow. For instance, in Fig. 2, there is clearly an observable rearrangement at $r/d \approx 17$, a region where the mean velocity is too small to measure easily. The impact on the rest of the profile is also observable, although simple quantitative characterizations, such as the widths, C^{-1} , are virtually indistinguishable within experimental error for 10 and 220 rotations ($3.2d$ and $2.7d$, respectively). The possibility of changes like those near $r/d \approx 17$ imply the existence of very long time scales in the system, similar to those that are observed in compaction [27,28,30]. These very long times appear to play a role in moderate but clearly observable variations in the velocity profiles over very long experiments.

We now sketch the qualitative properties of this system as we increase γ . Below γ_c , the sample is quiescent all the time. Thus at very low packing fractions, we expect that no motion will occur after initial transients (assuming, for example, a uniform initial packing). In particular, the disks are easily pushed away from the wheel, where after some rearranging, they remain without further contact. Just above a critical packing fraction γ_c the system is just strong enough to allow shearing indefinitely. The displacement of particles, and/or the formation of stress chains, occur at isolated and temporally fluctuating angular locations. For γ well above γ_c stresses are large, and chains appear in many places throughout the system. The displacement of particles occurs at many different angular positions simultaneously.

One of the key aspects of the present experiments is the exploration of packing fractions near γ_c . For $\gamma < \gamma_c$, disks are pushed away from the shearing wheel, and after transients, the systems remains at rest indefinitely. Just above γ_c , disks at a given position are sheared only intermittently, but once γ_c has been crossed, the disks will always be under shear somewhere in the system. For γ well above γ_c , the system is in the densely packed regime that is typical of usual gravitationally compacted 3D systems.

The range of γ studied was chosen so that at the lowest $\gamma \approx \gamma_c$, the disks were only rarely in contact with the shearing wheel, and at high γ the system was densely packed, with the innermost disks constantly in contact with the shearing wheel. Notably, only a small variation in γ , less than 4%, was sufficient to traverse this regime.

The transition at γ_c is related to Reynolds dilatancy. However, in the usual picture of Reynolds dilatancy, the system is under normal load, and significant shear stresses are needed to deform the system. At the yield point, the system then tends to dilate at the mechanically weakest point. In the present experiments, the system as a whole is actually quite

soft, easily sheared, and highly compressible. In order to distinguish the present case from the conventional picture, we will refer to the transition at γ_c as the softening (or strengthening) transition (ST).

In an ordinary 3D granular material, the corresponding γ_c is not generally accessible, because gravity compacts the material. This compaction occurs readily near γ_c , because the material is so highly compressible. Since there are no gravitational effects in this experiment, we can adjust the mean packing fraction, and hence use it as the control parameter, rather than the normal load.

There is one final aspect of these experiments that facilitates the observations of the ST, namely, the relative softness of the disks. To understand why this is important, we envision what would happen if we were to make the disks increasingly stiffer. We would expect to find that properties such as the mean stress would increase faster for γ increasing above γ_c , for increasingly stiffer disks. The rapid increase in mean stress above γ_c for stiff disks would make observations of the near- γ_c properties harder.

The precise experimental determination of γ_c is difficult because near γ_c , forces are weak, and changes occur intermittently over long times. The reason for this slow evolution is obvious on reflection. Although slow relaxation is observed for compaction [27,28], the phenomena here relate to the critical nature of the transition, rather than to the difficulty of rearranging the packing. Specifically, the packing in this case is highly compressible, as opposed to the long-time limit of the compaction case.

It is interesting, and perhaps not surprising, that γ_c is very close to the packing fraction for a square lattice, $\gamma_s = \pi/4 \approx 0.785$. By contrast, a hexagonally ordered packing of disks occurs for $\gamma_h = \pi/(2 \cdot 3^{1/2}) = 0.907$. Our system becomes stiff well below this packing fraction at a value comparable to those found for a random close packing of disks ($\gamma_{rcp} \approx 0.82$) [29]. There are analogous packing fractions for 3D systems. However, as noted above, in typical earth-bound experiments, gravity invariably leads to systems that have higher values of γ than the corresponding critical value, and it is very difficult to approach this transition.

B. Distributions for V_θ and S

We turn next to the velocity and spin distributions for $\gamma \geq \gamma_c$. The azimuthal velocities, V_θ/Ω , and particle spin, $S/(\Omega D/d)$, are particularly interesting. Distributions for V_θ/Ω and $S/(\Omega D/d)$ close to the shearing wheel are shown in Fig. 3 and their mean values versus r/d in Fig. 4 for different values of $\tau = 2\pi\Omega^{-1}$. All distributions have been normalized to unity, and the packing fraction, $\gamma = 0.788$, is in the midrange of the values studied here.

The mean of V_θ/Ω as a function of r/d , Fig. 4, shows a roughly exponential profile corresponding to a shear zone with a width of a few d . By $r/d = 7$, the data have reached the noise level. This is consistent with previous observations for quasistatic flow [7,22]. Although the profile is nearly exponential in distance from the wheel, there is also the suggestion of some downward curvature when V_θ/Ω is viewed semilogarithmically. The solid curve in Fig. 4 shows a fit of $\ln(V_\theta/\Omega)$ to $-A - B(r/d) - C(r/d)^2$ in the range $0 < r/d < 6$. The fit coefficients are $A = 0.503 \pm 0.148$, $B = 0.417$

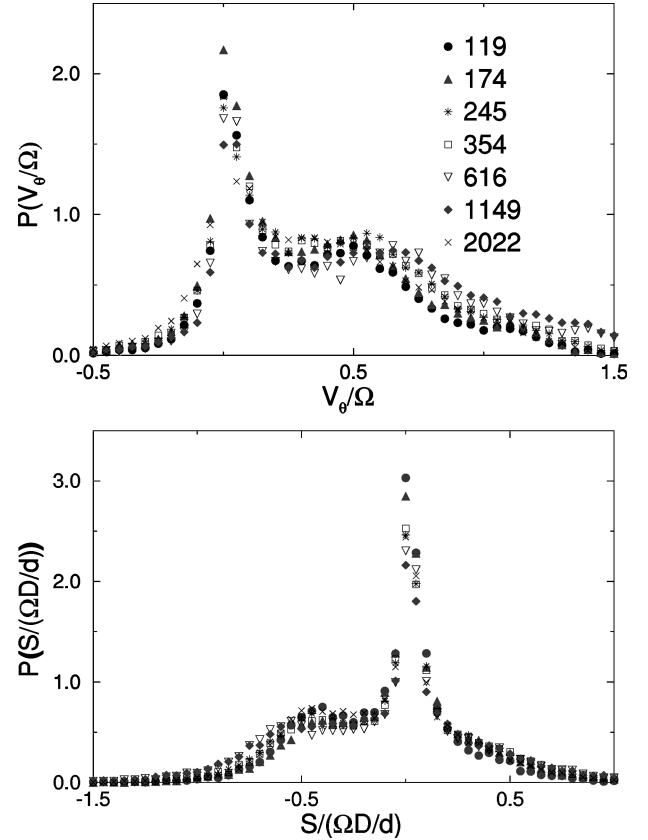


FIG. 3. Normalized azimuthal velocity and spin distributions close to the inner wheel for different rotation times, for $\gamma = 0.788$. Data are taken from radii $0 < r/d < 1$. The symbols refer to different values of the rotation time τ in seconds. If there were perfect rate invariance, these distributions would collapse perfectly.

± 0.096 , and $C = 0.105 \pm 0.013$. The quoted errors reflect the statistical uncertainty. The second-order correction is relatively weak, and becomes comparable to the leading term only for $r/d \approx 6$. The characteristic decay length in this case, $B^{-1} = 2.4d$, is somewhat smaller than the corresponding decay length for the density profiles. Presumably, the reason for the more rapid decay for V_θ than for γ is the rapid drop in disk mobility with increasing γ . The approximately exponential form for V_θ/Ω is interesting, since it suggests the possibility that disks past the first few layers may eventually move, but only after exponentially long-time scales.

The mean profiles for $S/(\Omega D/d)$ are also interesting. The disks nearest to the inner wheel rotate backwards on average—i.e., in the direction opposite to the wheel rotation. However, the next layer rotates in same direction as the wheel on average. These oscillations in the mean spin damp very quickly with distance from the wheel. In order to determine how fast the spin decays to zero, we fit the spin profile to $S/(\Omega D/d) = A \exp[-B(r/d)] \cos(\pi r/d + \phi)$. Here, the key fit coefficients are $A = 0.760 \pm 0.116$, $B = 1.67 \pm 0.19$, and $\phi = 0.790 \pm 0.080$. Here, the errors represent the statistical uncertainty. Again the second-order correction is very small. The characteristic length in this case is just above $0.5d$, which is even faster than the velocity decay. This is likely related to the fact that the spin of the disks in a given layer is driven in one direction by neighboring disks in the next-closest layer to the wheel, while at the same time impeded by

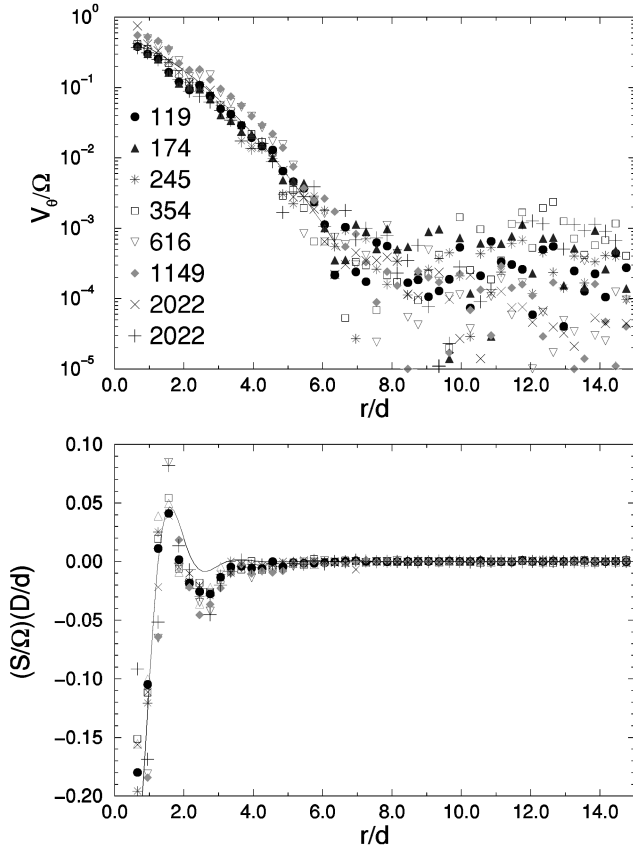


FIG. 4. Mean azimuthal velocity and mean spin for different rotation rates at $\gamma=0.788$. The symbols refer to different values of the rotation time τ in seconds. Two sets of data at $\tau=2022$ sec show that deviations between the different rates are comparable to reproducibility from run to run at the same rate. The solid lines correspond to the fits described in the text.

the neighboring disks that lie one layer further from the wheel.

An inspection of Fig. 4 shows that the data for different τ for the means of both V_θ/Ω and $S/(\Omega D/d)$ do not fall exactly on top of each other. For a given Ω , the data are smooth in r , so that the variability in scaled velocity is not simply experimental uncertainty in determining V_θ .

This suggests a breakdown of the rate invariance and the quasistatic limit. However, the reasons for the noncollapse of the data are more subtle. Specifically, there is no clear trend in the data for either of these quantities with increasing Ω . Although the widths of the distributions, are large, the smooth variation of the mean velocity with r again suggests that this alone cannot account for the departures from scaling. At this point, we believe that departure from rate independence in the mean profiles is related to relatively small fluctuations in the packing profiles over long times—i.e., after the wheel has moved many disk diameters. Thus, we might expect that if data were obtained over observation times much longer than what we have used, rate independence might well be seen, although the widths of the distributions would be little changed. Put differently, our results suggest that there are long time scales over which small packing adjustments can occur, and that these adjustments affect the kinematic properties of the system. We expect to pursue even longer time scales in future experiments.

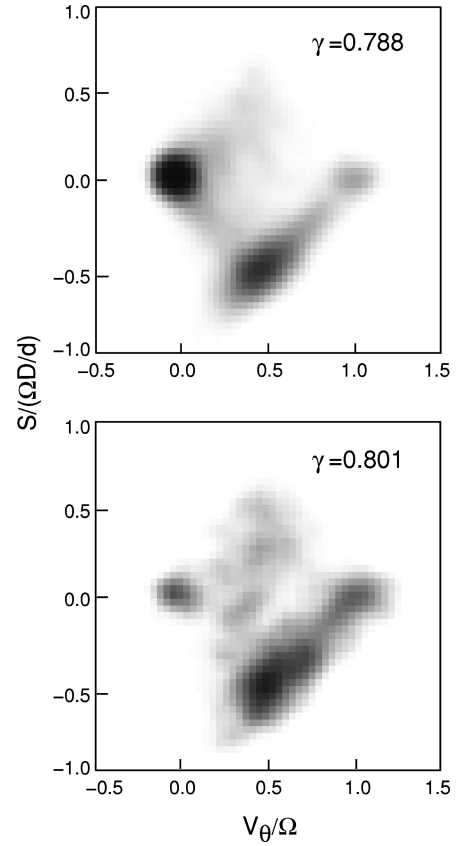


FIG. 5. Gray scale representation of the 2D probability density for V_θ/Ω and $S/(\Omega D/d)$ for $0 < r/d < 1$. Data are shown for two indicated values of γ .

The distributions $P(V_\theta/\Omega)$ and $P(S/(\Omega D/d))$ for moderate γ reveal additional interesting features. $P(V_\theta/\Omega)$ for the innermost layer, Fig. 3, shows that there is some motion in the negative direction, i.e., for $V_\theta/\Omega < 0$ and in the positive direction for $V_\theta/\Omega > 1$. These types of motion occur because disks slip backwards or forwards as a chain fails. There is a large peak at $V_\theta/\Omega = 0$ that corresponds to disks that remain at rest. The next-largest feature is at $V_\theta/\Omega \approx 0.5$, corresponding to disks that move at approximately 1/2 the wheel speed, and there also appears to be some structure at $V_\theta/\Omega \approx 1.0$. These various features lead to a complex distribution for V_θ/Ω reflecting a combination of slip and non-slip events, as discussed below. However, for practical purposes, a fit of the distribution $P(V_\theta/\Omega)$ to three Gaussians centered at 0.0, 0.5, and 1.0 leads to a good quantitative characterization of the data shown in Fig. 3.

The distribution for $S/(\Omega D/d)$ near the shearing wheel shows qualitatively similar structure except that it occurs for negative S , corresponding to the backward spin seen in the mean profile. In addition, there are only two peaks for the spin distribution. However, a fit to two Gaussians for the spin is not quite as good as either a two- or three-Gaussian fit to the V_θ distribution.

A key understanding of the structure of the one-variable distributions for V_θ and S comes from Fig. 5, which shows two examples, for two different packing fractions, of the two-variable distribution $P(V_\theta/\Omega, S/(\Omega D/d))$ for grains within one particle diameter of the wheel. Here, $P(V_\theta/\Omega, S/(\Omega D/d))$ is coded in gray scale (dark is high probability density.) Figure 5 shows that there are two dis-

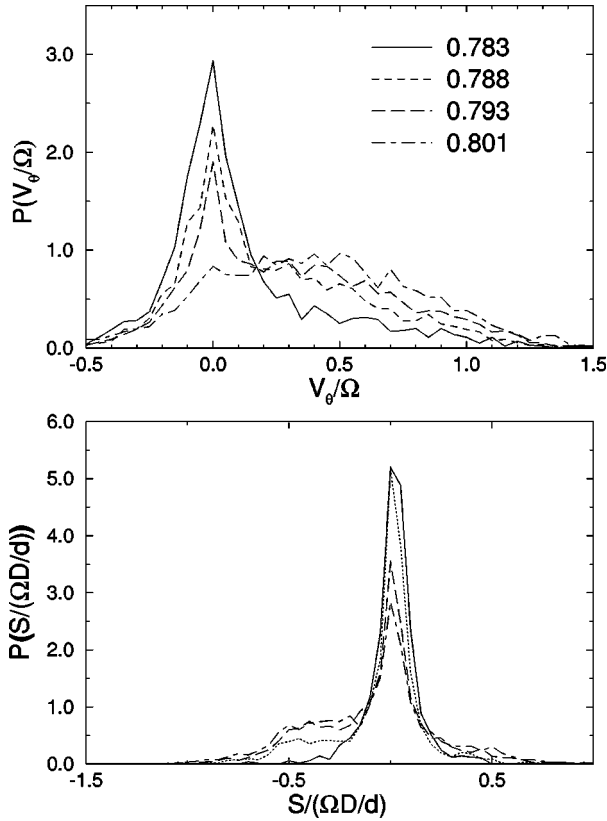


FIG. 6. Azimuthal velocity and spin distributions close to the inner wheel. Data are taken from radii $0 < r/d < 1$. Different lines are for different packing fractions γ , as noted.

tinct features corresponding to two qualitatively different processes. Which of these processes is most important changes with increasing γ . One of these features, centered around (0,0), corresponds to a state where disks are essentially at rest, without either translation or spin. The other is clustered around a line $V_\theta/\Omega = 1 + S/(\Omega D/d)$ that corresponds to nonslip motion of grains relative to the wheel, with much of the weight near (0.5, -0.5). By no slip, we mean that particles execute a combination of backwards rolling and translation such that the wheel surface and the disk surfaces remain in continued contact. The peak at $V_\theta/\Omega = 0$ is strong for lower γ , but it has almost vanished at $\gamma = 0.801$, and the data fall around the no slip line. Thus the transition at γ_c can also be thought of as one in which slip at the shearing surface is replaced by nonslip in a continuous way.

In Fig. 6 we show quantitative data for the distributions for various γ 's. With increasing γ , the peaks in $P(V_\theta/\Omega)$ and $P(S/(\Omega D/d))$ near zero weaken, and the corresponding regions with negative spin and nonzero V_θ grow. A surprising feature is that the part of the distribution satisfying nonslip does not extend to velocities much lower than $V_\theta/\Omega \approx 0.5$. This may be related to specific properties of this system, such as frictional or geometric properties. We will pursue this point in future experiments.

The distributions narrow rapidly with distance away from the wheel, and approach an instrumentally sharp distribution centered around $V_\theta = 0$. In the large- r regime, past the first seven layers, the distribution width reflects primarily experimental errors from finite pixel size, tape registry errors, etc. In this nearly stationary regime, rolling of the disks is im-

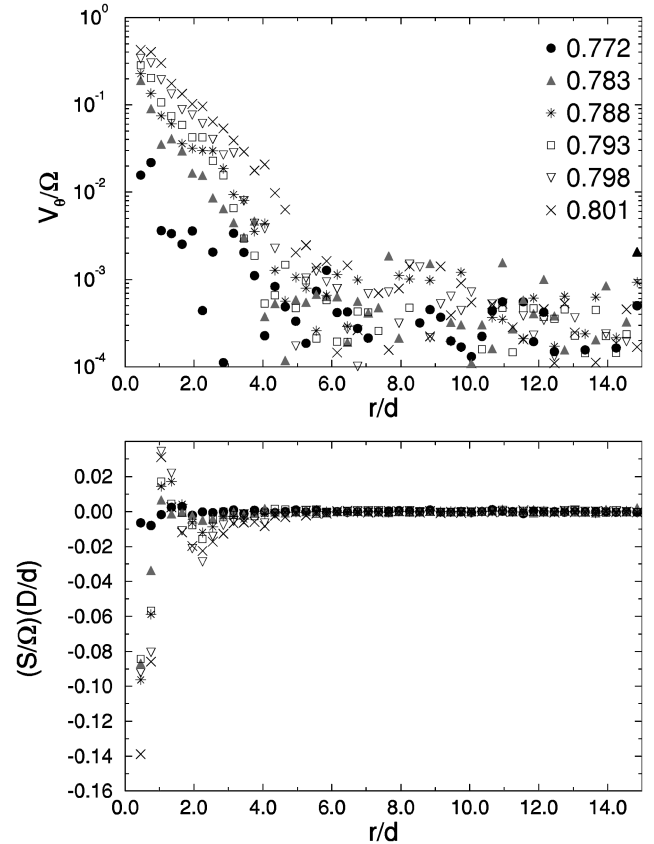


FIG. 7. Mean azimuthal velocity and mean spin. Different symbols are for different γ .

possible, and S is no longer an important variable. However, there may well be some fast-slipping events that are beyond the resolution of the imaging equipment used here.

From the above discussion, it is clear that changing the packing fraction must change not only the distributions, but also the mean properties. In Fig. 7 we show quantitative data for the profiles for several values of γ . We average data for different values of Ω to obtain statistics from almost 10^6 data points. The V_θ/Ω profiles show a roughly exponential decay with a comparable characteristic length for all γ . The amplitude of the exponential term grows steadily from zero as γ increases above γ_c . The profile for $S/(\Omega D/d)$ also evolves in qualitatively the same manner with γ . This evolution of the spin and velocity profiles with γ is, of course, tied intimately to the density profiles, Fig. 8.

IV. CONCLUSIONS

To conclude, this work is an exploration of the kinematic statistical properties for slow 2D granular shear flow. We have focused on the transition to shearing that first occurs for packing fractions greater than a critical value, $\gamma_c \approx 0.77$. This transition has some features reminiscent of a second-order thermodynamic phase transition, including the existence of an order parameter, critical slowing down, and large compressibility.

With increasing γ , the following qualitative behavior occurs. Below γ_c , the disks can remain indefinitely at rest. Just above γ_c , the disks move very slowly, so that necessarily, the system shows critical slowing down as $\gamma \rightarrow \gamma_c$ from above. This slow behavior is qualitatively different from the

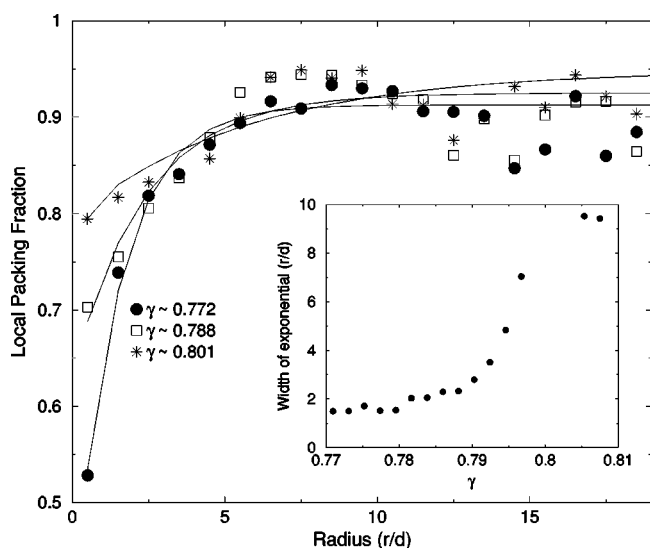


FIG. 8. Steady-state density profiles for different values of γ . Solid lines are exponential fits (see text). Inset: The exponential width of the steady-state profiles vs the overall packing fraction.

slow time that appears in densely packed systems where rearrangement of the grains becomes increasingly more difficult with time. Of course, rearrangements of this type also occur particularly at dense packings, and influence the statistical and mean properties of the flow on relatively long time scales.

The density, and azimuthal velocity obey roughly expo-

ponential profiles with distance from the wheel, and these profiles grow as γ rises above γ_c . The spin profiles show interesting oscillations and disks next to the wheel have a high probability of rotating backwards. This feature is particularly clear in the bimodal distributions for S and V_θ ; these show that the transition near γ_c is characterized by a change from complete slipping to increasingly nonslip dynamics. The latter behavior is qualitatively similar to the usual nonslip condition for conventional fluids, except that here the rolling component must also be considered. These distributions also show forward and backward slipping events at velocities less than 0, and greater than the wheel velocity.

There are a number of other interesting aspects of this system that we will describe elsewhere [13]. These include the force distributions, and other measures associated with dynamical properties.

ACKNOWLEDGMENTS

C.T.V. and R.P.B. are indebted to the École Supérieure de Physique et Chimie Industrielle, PMMH, where parts of this work were carried out. We particularly appreciate interactions with Professor Hans Herrmann, as well as useful comments by Joshua Socolar, David Schaeffer, Stéphane Roux, Eric Clément, Jean Rajchenbach, and P.-G. de Gennes. The work of D.W.H. and R.P.B. was supported by the National Science Foundation under Grant Nos. DMR-9321791 and DMS-9504577, and by NASA under Grant No. NAG3-1917. The work of C.T.V. was supported by the Danish Science Foundation (Statens Naturvidenskabelige Forskningsråd).

-
- [1] O. Reynolds, *Philos. Mag.* **5**, 50, 496 (1885).
 [2] R. A. Bagnold, *Proc. R. Soc. London, Ser. A* **225**, 49 (1954).
 [3] J. B. Knight, *Phys. Rev. E* **55**, 6016 (1997).
 [4] R. M. Nedderman and C. Laohakul, *Powder Technol.* **25**, 91 (1980).
 [5] T. G. Drake, *J. Geophys. Res.* **95**, 8681 (1990).
 [6] S. B. Savage and K. Hutter, *J. Fluid Mech.* **199**, 177 (1989).
 [7] O. Pouliquen and R. Gutfraind, *Phys. Rev. E* **53**, 552 (1996).
 [8] A. Ngadit and J. Rachenbach, *Phys. Rev. Lett.* **80**, 273 (1998).
 [9] H. J. Herrmann, A. N. B. Poliakov, and S. Roux, *Fractals* **3**, 821 (1995).
 [10] H. M. Jaeger, S. R. Nagel, and R. P. Behringer, *Phys. Today* **49**, 32 (1996); *Rev. Mod. Phys.* **68**, 1259 (1996).
 [11] *Powders and Grains 97*, edited by R. P. Behringer and J. T. Jenkins (Balkema, Rotterdam, 1997).
 [12] *Physics of Dry Granular Media*, Vol. 350 of *NATO Advanced Study Institute Series E: Applied Sciences*, edited by H. J. Herrmann, J. P. Hovi, and S. Luding (Kluwer, Amsterdam, 1998).
 [13] D. W. Howell, C. T. Veje, and R. P. Behringer (unpublished).
 [14] For a review see R. Jackson, in *Theory of Dispersed Multiphase Flow*, edited by R. Meyer (Academic, New York, 1983).
 [15] K. H. Roscoe, *Geotechnique* **20**, 129 (1970).
 [16] H.-B. Mühlhaus and I. Vardoulakis, *Geotechnique* **37**, 271 (1987).
 [17] J. F. Carr and D. M. Walker, *Powder Technol.* **1**, 369 (1967).
 [18] S. B. Savage and S. McKeown, *J. Fluid Mech.* **127**, 453 (1983).
 [19] B. Miller, C. O'Hern, and R. P. Behringer, *Phys. Rev. Lett.* **77**, 3110 (1996).
 [20] S. B. Savage, *Adv. Appl. Mech.* **24**, 289 (1984).
 [21] E. Azana, F. Chevoir and P. Moucheron, in *Powders and Grains 97* (Ref. [11]).
 [22] H. Buggisch and G. Löffelmann, *Chemical Engineering and Processing* **26**, 193 (1989).
 [23] C. S. Campbell and C. E. Brennen, *J. Fluid Mech.* **151**, 167 (1985).
 [24] H.-J. Tillemans and H. J. Herrmann, *Physica A* **217**, 261 (1995).
 [25] S. Schöllmann, S. Luding, and H. J. Herrmann (unpublished).
 [26] C. T. Veje, D. W. Howell, R. P. Behringer, S. Schöllmann, S. Luding, and H. J. Herrmann, in *Dry Granular Media* (Ref. [12]).
 [27] J. B. Knight, C. G. Fandrich, C. N. Lau, H. M. Jaeger, and S. R. Nagel, *Phys. Rev. E* **51**, 3957 (1995).
 [28] E. Ben-Naim, J. B. Knight, and E. R. Nowak, *J. Chem. Phys.* **100**, 6778 (1996).
 [29] L. Rouillé, J.-M. Missiaen, and G. Thomas, *J. Phys.: Condens. Matter* **2**, 3041 (1990).
 [30] Edmund R. Nowak, J. B. Knight, E. Ben-Naim, H. M. Jaeger, and S. R. Nagel, *Phys. Rev. E* **57**, 1971 (1998).